Open Archive TOULOUSE Archive Ouverte (OATAO)

Analysis and Modeling of Linear-Switched Reluctance for Medical Application

Jean-Francois Llibre [1,2,*], Nicolas Martinez [3], Pascal Leprince [4] and Bertrand Nogarede [1,2]

[1]   University of Toulouse, INPT, UPS; ENSEEIHT, 2 rue Charles Camichel, BP 7122, F-31071
     Toulouse cedex 7, France; E-Mail: bertrand.nogarede@laplace.univ-tlse.fr
[2]   National Center for Scientific Research (CNRS); LAPLACE; F-31071 Toulouse, France
[3]   Novatem Simplified joint-stock company (SAS); ENSEEIHT, 27 rue d'Aubuisson F-31071
     Toulouse cedex 7, France; E-Mail: nicolas.martinez@novatem-sas.com
[4]   Cardiology Institute, Pitié-Salpêtrière Hospital, 47-83 Bd de l'Hôpital, 75651 Paris Cedex 13,
     France; E-Mail: pascal.leprince@psl.aphp.fr

*   Author to whom correspondence should be addressed; E-Mail: llibre@laplace.univ-tlse.fr;
    Tel.: +33-5-3432-2375; Fax: +33-5-6163-8878.

Abstract: This paper focuses on the analysis, the modeling and the control of a linear-switched reluctance motor. The application under consideration is medical, and the actuator is to be used as a left ventricular assist device. The actuator has a cylindrical or tubular shape, with a mechanical unidirectional valve placed inside the mover, which provides a pulsatile flow of blood. The analytical expression of the effort based on the linear behavior of the actuator is given. The identification of the characteristics of the prototype actuator and the principle of position control is performed. A modeling of the actuator is proposed, taking into account the variation of inductance with respect to the position. The closed-loop position control of the actuator is performed by simulation. A controller with integral action and anticipatory action is implemented in order to compensate the effects of disturbing efforts and tracking deviations. Moreover, a magic switch is performed in the controller to avoid overshoots. The results show that the closed-loop response of the actuator is satisfactory.

Keywords: switched reluctance; modeling; linear actuator; position control; medical application

1. Introduction

Heart failure is one of the most common diseases in developed countries. In most of the cases, a left ventricular assist device (LVAD) is used to treat patients. The LVAD assists the failing left ventricle by providing an additional flow of blood in the body [1].

At the beginning of cardiovascular surgery, mechanical circulatory support (MCS), which is a pneumatic pump, mimics the function of the heart by providing a pulsatile flow of blood. The major limitations are the sheer size of the pump, limited mobility, because of a large drive console, and the need for constant anticoagulation solutions [1]. The latest generation of MCS consists of miniature rotary pumps providing a continuous flow of blood. One can cite the Jarvik 2000, the MicroMed DeBakey and the Heart Mate II, which are axial electromagnetic pumps, including a motor and a turbine [2]. They increase the autonomy of the patient and improve overall life comfort. The success of these devices is limited by thromboembolic events and pump thrombosis. Moreover, the implications of continuous flow conditions over long periods remain unclear to the medical and scientific community [3].

To prevent thrombosis, we propose to study a pulsatile flow pump for *in vivo* tests on pigs. The physiological needs are a pressure of 120 mmHg, a flow of 3 liters/min and a heart rate of 120 bpm (beats per minute). The actuator chosen is a linear-switched reluctance motor (LSRM). The stator and the mover have a cylindrical or tubular shape, with a mechanical unidirectional valve placed inside the mover. This pump, called Pulsamag, incorporates the valve and pump functions.

The aims of the paper are to describe the characteristics and the modeling of this LSRM structure in order to control it and then to show the applicability of the motor for LVAD. The organization of the paper is as follows: the topology of the proposed LSRM and its basic operational principles are described in Section 2; Section 3 gives the dimensional characteristics of the motor; Section 4 presents the modeling of the motor; and Section 5 describes the conclusions and perspectives of the work.

2. Proposed Concept of the LVAD

2.1. Presentation of the Actuator

For the application considered, the cylindrical LSRM is a good candidate. Its structure is simple and robust, and the mover part has no windings, as in [4,5]. It consists of a hollow, mobile ferromagnetic cylinder with transversal slots and an outer cylindrical stator containing a number of identical phase sets. Each set consists of a magnetic core, formed by two discs and a ring and an enclosed solenoid winding. In the same manner, a six phase cylindrical LSRM has been developed for circulatory heart assistance [6].

The actuator studied is called Pulsamag and is presented in [7]; it has a mechanical unidirectional valve fixed inside the cylindrical mover. This aortic valve, made by St. Jude Medical, has a diameter of 25 mm and allows blood circulation. As shown in Figure 1, the cylindrical LSRM studied is composed of a stator with four phases and eight coils (two coils per phase) and a tubular mover. Each set of the stator is separated from its neighbor by a non-magnetic ring. Phase number 1 is composed of coils, numbers 1 and 5. The other coils and phases are numbered in the same way.

The coils are sequentially excited in order to create a magnetic field moving from one end to the other. Then the cylindrical magnetic mover performs an oscillatory movement. The closed aortic valve

pushes the fluid in the flow direction, and when the cylinder comes back to its initial position, the valve is opened, so as not to interact with the fluid.

Figure 1. (**a**) Basic structure of Pulsamag; (**b**) Design of Pulsamag.

(**a**)   (**b**)
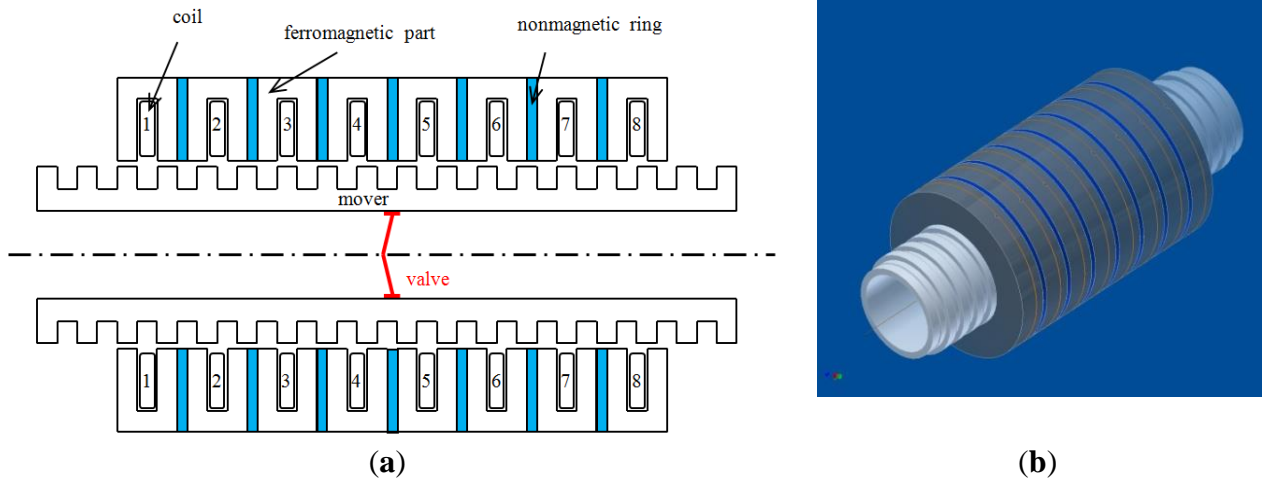
In this low speed application, because of low eddy current losses, the magnetic core does not have to be made of laminated steel. Moreover, due to the cylindrical shape, the normal forces are neutralized. The other advantages of this kind of actuator are its reliability, its simplicity of implementation, its ability to generate a linear motion directly (without mechanical processing), *etc.* Its disadvantages include low efficiency, due to a loss of joules that increases proportionally to the desired mechanical effort generated, and the difficulty of guiding the mover part to ensure a constant air gap.

2.2. Kinetic Characteristics of the Motor

According to [7], the stroke of the St. Jude Medical valve and the mover is:

$$L = \frac{10^3}{6} \frac{Q}{Sf}$$
(1)

where L is the stroke of the mover in mm, Q is the desired flow in L/min, S is the section of the valve in cm² and f is the desired frequency in Hz.

The thrust of the mover is:

$$F = \frac{PS}{10}$$
(2)

where F is the thrust in N and P is the pressure in kPa.

The physiological needs for a ventricular assist device are a flow of 3 L/min and a pressure of 120 mmHg (16kPa) under a frequency of 2 Hz (120 bpm). Therefore, with a 25 mm diameter valve, the stroke is $L \cong 50$mm and the thrust is $F \cong 8$ N.

According to Equation (1), the control of the position of the mover at a given frequency will fix the blood flow. By setting a value of supply voltage, a current is injected in each phase. Thus, the driving force required is produced and, in accordance with Equation (2), blood pressure is imposed.

3. Dimensional Characteristics of the LVAD

3.1. Prototype Dimensions and Characteristics

From the actuator presented in Figure 1, it can be noted that each phase set forms an independent magnetic circuit thanks to the non-magnetic ring. The phase set or basic pattern of the actuator is presented in Figure 2(a). It is formed of a stator ferromagnetic part with one slot (with a coil) and two teeth and a ferromagnetic mover part with one slot (without a coil) and two teeth. When the coil is excited, the stator teeth and the mover teeth tend to be aligned in order to maximize the magnetic flux.

The radial dimensions (y-axis) are: stator yoke thickness, e_{sy}, stator tooth length, h_{st}, mover tooth length, h_{mt}, mover yoke thickness, e_{my}, external radius, R_{ext}, air gap radius, R_g, and valve radius, R_v. The axial dimensions (x-axis) are: tooth width, a, and slot width, b.

Figure 2. (**a**) Basic pattern; (**b**) Picture of Pulsamag prototype.

(**a**)   (**b**)
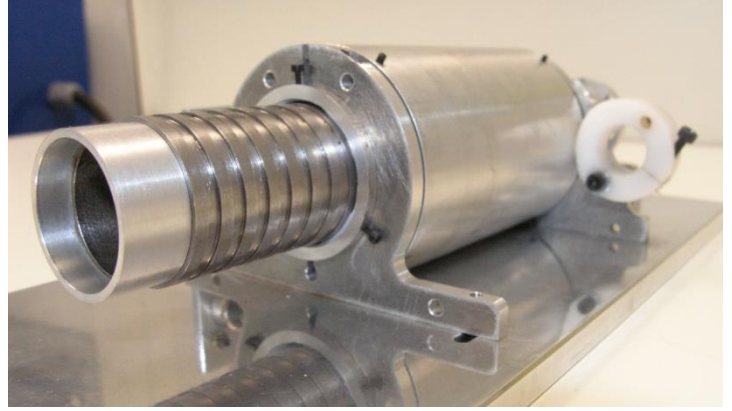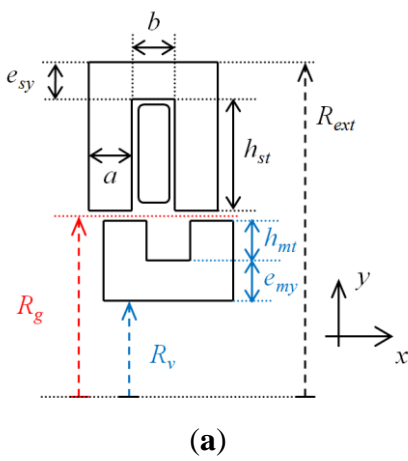
The sizing and the two-dimensional finite element analysis of the actuator are presented in [7,8]. In order to ensure smooth functioning, we chose the tooth pitch of the stator, λ_s and the tooth pitch of the mover, λ_m, to be equal, the tooth width, a, and the slot width, b, to be equal, too:

$$\lambda_s = \lambda_m = \lambda = a + b \ \ \text{with} \ \ a = b \tag{3}$$

We can notice in Figure 1(a) that to separate two basic patterns, a non-magnetic ring has to be inserted. Its thickness value, c, depends on the number of phases and on the tooth pitch values. For the Pulsamag prototype, we chose to make the thickness of the non-magnetic ring, c, half that of the tooth width, a.

The stroke of the actuator depends on: the tooth pitch length, λ, the non-magnetic ring thickness, c, the phase number, m, and the coils per phase number, n. To increase the stroke for a given elementary pattern dimensions, we can increase m and/or n. By supplying several coils in series ($n \neq 1$), both the stroke and the thrust increase.

The total length of the stator, L_{sT}, is given by:

$$L_{sT} = mn(2a + b) + c(mn - 1) \tag{4}$$

The total length of the mover, L_{mT}, depends on the desired stroke, L, and is given by:

$$L_{mT} \geq L + L_{sT} \tag{5}$$

By assuming a linear model of the basic pattern, the analytical expression of the traction or propulsion force can be obtained using the principle of conversion of energy [9,10] and by neglecting the magnetic field in the iron relative to that in the air gap [5,8]. According to [8], the expression of the total expected thrust F_{xT} is given by:

$$F_{xT} = n \frac{\mu_0 \pi}{2} \frac{R_g}{g} (Ni)^2 \tag{6}$$

where Ni is the magnetomotive force (mmf) and g the length of the air gap.

It is to be noted that the lateral force will be high if the air gap length, g, is low, and the air gap radius, R_g, is high. Moreover, increasing the mmf, Ni leads to an increase of the thrust, but also a proportional increase in copper loss (square increase).

The actuator presented in Figure 1 has $m = 4$ phases and $n = 2$ coils per phase. The first phase is composed of coils 1 and 5 in series, and the other phases are formed and numbered in the same way. Supplying the phases in order 1-2-3-4 by a four-phase current system leads to a leftward shift, whereas the reverse sequence. 4-3-2-1. leads to a rightward shift. The distance covered by the mover when switching from one coil to the next is the mechanical step:

$$\lambda_p = \frac{\lambda}{m} = |b - c| \implies \lambda_p = \frac{\lambda}{4} = \frac{a}{2} = c \tag{7}$$

The prototype dimensions and a picture of the LSRM are given, respectively, in Table 1 and in Figure 2(b).

Table 1. Prototype dimensions.

Name	Abbreviation	Value (mm)
Valve radius	R_v	12.5
Mover yoke thickness	e_{my}	2
Mover tooth length	h_{mt}	1.5
Air gap length	g	0.2
Air gap radius	R_g	16.1
Stator tooth length	h_{st}	9
Stator yoke thickness	e_{sy}	1.5
External radius	R_{ext}	26.7
Tooth width	a	2.9
Slot width	b	2.9
Non-magnetic ring thickness	c	1.45
Total length of the stator	L_{sT}	80
Total length of the mover	L_{mT}	140

For the application considered, the desired stroke and the thrust are, respectively, 50 mm and 8 N. According to the above dimensions, the stroke is available.

The winding characteristics of the prototype are given in Table 2.

Table 2. Winding characteristics.

Name	Abbreviation	Value
Number of phases	m	4
Number of coils per phase	n	2
Number of turns per slot	N	155
Turn diameter	Φ_{turn}	0.335 mm
Slot area	$A_{slot} = bh_{st}$	26.1 mm²
Coil area	$A_{coil} = N\pi\Phi_{turn}^{2}/4$	13.66 mm²
Slot fill factor	$k_{fill} = A_{coil}/A_{slot}$	52.30%

The expression of the mmf, Ni, in terms of the previous areas expressed in mm² and the current density, J, expressed in A/mm², is:

$$Ni = A_{coil}J = k_{fill}A_{slot}J \tag{8}$$

Therefore, for a current supply of $i = 1$ A corresponding to a mmf of $Ni = 155$ At and a current density in the coil, $J = 11.3$ A/mm², the analytical thrust using Equation (6) is equal to 7.6 N. This value is close to that desired for the application. However, it should be remembered that the analytical expression assumes a linear operation, an independence of each magnetic circuit associated with each coil (due to the non-magnetic ring) and a null magnetic field in the iron relative to that in the air gap.

By measurements, it was determined that the prototype had the parameters and characteristics given in Table 3.

Table 3. Prototype characteristics.

Characteristic	Value
Mass of the mover	$m = 270.8$ g
Static dry friction force	$f_s = 1.75$ N
Winding resistance (average value)	$R = 8.5\ \Omega$
Unaligned Position inductance (average value)	$L_u = 34.1$ mH
Aligned Position inductance (average value)	$L_a = 44.6$ mH
Winding inductance (average value)	$L = 39.4$ mH
Rate of change of inductance (average value)	$\Delta L/\Delta x = 10/2.9$

3.2. Input-Output Characteristics

The output power, P_{out}, is given as the product of the kinetic thrust, F_{xT}, and average speed, $\bar{v}$, as:

$$P_{out} = F_{xT} \cdot \bar{v} \tag{9}$$

By supplying one phase after the other, the average speed can be expressed according to the desired frequency, f (*i.e.*, desired heart rate) and the desired stroke, L, as:

$$\bar{v} = L \cdot f \tag{10}$$

In this low speed application (the frequency is low, typically under 3 Hz), the iron losses can be neglected compared to the copper losses. Therefore, the efficiency, η, is given by:

$$\eta = \frac{P_{out}}{P_{out} + P_J} \tag{11}$$

where P_J are the Joule losses.

The Joule losses for one energized phase (constituted of n coils) are:

$$P_J = nRi^2 \tag{12}$$

where R is the winding resistance, which can be expressed according to the electrical resistivity of copper, ρ, the winding average length of turn, l_t, and its cross section, A_t:

$$R = \rho \frac{l_t}{A_t} N = \rho \frac{l_t}{A_{coil}} N^2 = \rho \frac{l_t}{k_{fill} A_{slot}} N^2 \tag{13}$$

where:

$$l_t = \pi \left[\left(R_{ext} - e_{sy} \right) + \left(R_g + \frac{g}{2} \right) \right] \tag{14}$$

and:

$$A_{slot} = bh_{st} = b \left[\left(R_{ext} - e_{sy} \right) - \left(R_g + \frac{g}{2} \right) \right] \tag{15}$$

Finally, the Joule losses can be expressed by:

$$P_J = \frac{n\pi\rho}{bk_{fill}} \frac{\left[\left(R_{ext} - e_{sy} \right) + \left(R_g + \frac{g}{2} \right) \right]}{\left[\left(R_{ext} - e_{sy} \right) - \left(R_g + \frac{g}{2} \right) \right]} (Ni)^2 \tag{16}$$

One dimensioning factor for switched reluctance motors is the maximization of the mean torque per copper loss. In [5], this optimization gives the following result (by neglecting the dimension, $g/2$, to the R_g dimension in the previous expression):

$$\frac{d \frac{F_{xT}}{P_J}}{dR_g} = 0 \quad \Rightarrow \quad R_g \cong \left(\sqrt{2} - 1 \right) \cdot \left(R_{ext} - e_{sy} \right) \tag{17}$$

If we neglect the stator yoke thickness, e_{sy}, compared to the external radius, R_{ext}, the optimum ratio is 0.4 between the air gap radius, R_g, and the external radius, R_{ext}. For our prototype, the external radius, R_{ext}, according to Equation (17), will be larger than 31 mm, considering the radius valve value, R_v, which is equal to 12.5 mm. In order to limit the sheer size of the actuator (external radius inferior to 30 mm) and the mass of the mover, we have chosen the dimensions given in Table 1.

By supplying one phase after the other, we can calculate the output power, the input power and the efficiency at different frequencies (*cf.* Figure 3). As mentioned previously, because the frequency is low, iron losses are negligible. The Joule losses are considered constant and equal for each phase supplied. We can notice that the efficiency of the LSRM is very low, as in [6]. In this medical application, efficiency is not the main design criterion. The choice of this architecture is guided by the application.

Figure 3. Input power, output power and efficiency *versus* frequency.
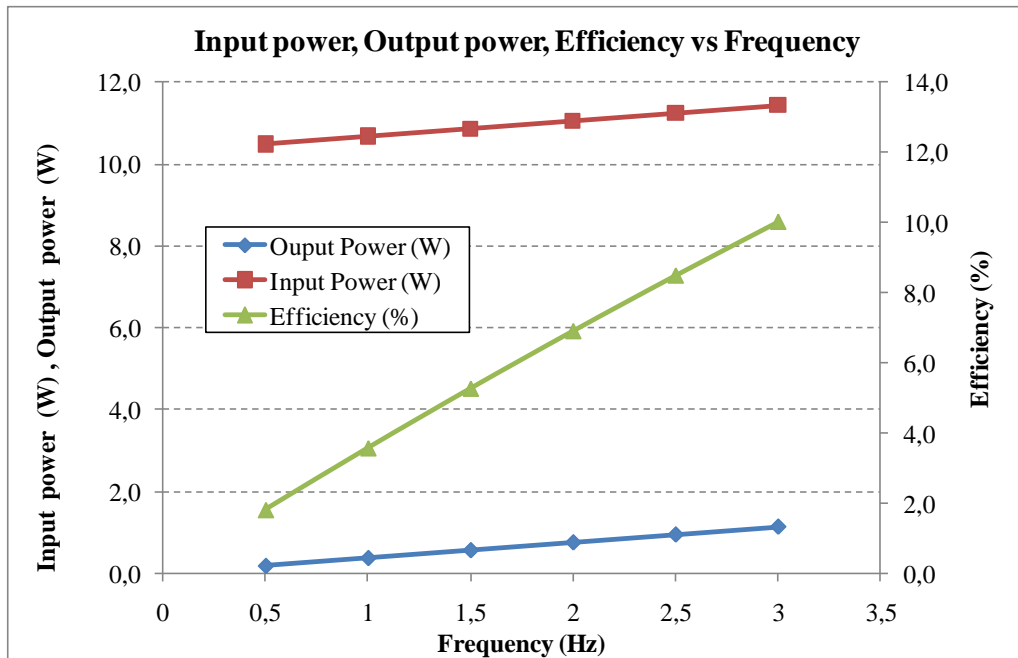
4. Control Principle

4.1. Open Loop Control of the Motor

4.1.1. Presentation

The motor is controlled using a dSPACE system with a DS1005 PWM card and a DS2202 acquisition card. A Mitutoyo LGF-550L position sensor with the EH10P signal conditioner is used to obtain the real position of the mover. The power supply of the prototype has been developed by the Novatem SAS Company and consists of four independent H-bridges (one H-bridge per phase). Figure 4 shows the test bench of the Pulsamag prototype.

In this pump application, the functioning of the motor requires a back and forth motion. The motor is to be controlled in position with a sinusoidal variation of the position:

$$x = \hat{X} \sin(\omega t) = \hat{X} \sin(2\pi f t) \tag{18}$$

where $\hat{X}$ is equal to half the desired stroke and *f* is the operating frequency equal to the desired cardiac frequency (*cf.* Equation (1)).

Figure 4. Test bench of Pulsamag prototype.
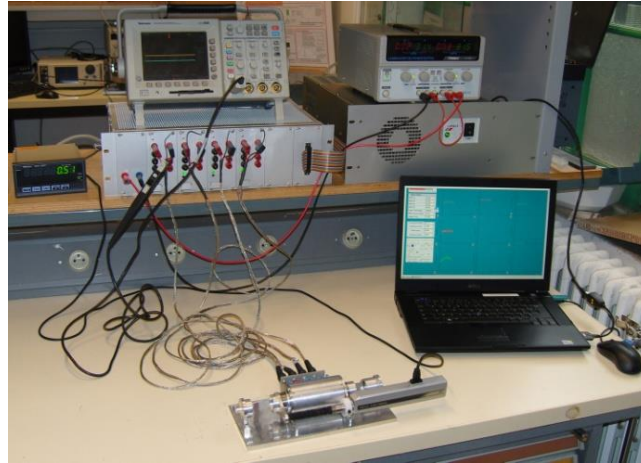
The control of the motor has been developed using Matlab Simulink software in discrete mode with a sampling period: $T_e = 100$ µs. The real position of the mover, called x_m, measured by the sensor position, will be compared to the reference sinusoidal signal, x, of Equation (18). Figure 5 shows the open loop control of the motor. Concerning the use of Matlab Simulink and dSPACE tools for the control of SRM, we can cite the works [11,12] for variable speed pumping applications.

Figure 5. Open loop control of the motor. PWM, pulse-width modulation.
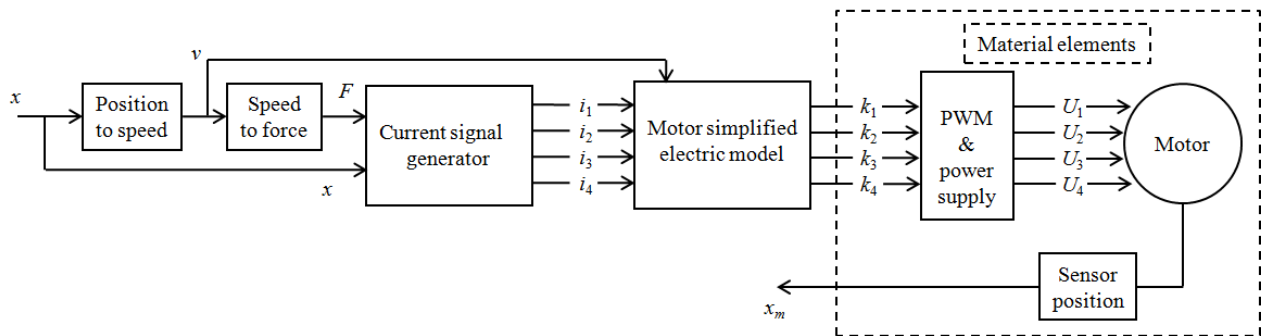
The elements that are inside the dotted box in Figure 5 are the material elements of the control. In the "PWM & power supply" block, the DS1005 pulse-width modulation (PWM) card generates the PWM signals needed for the Novatem SAS power supply. This provides voltages, U_1 to U_4, to the motor. In the "Sensor position" block, the DS2202 card is used to retrieve the real position of the mover, x_m, measured by the Mitutoyo sensor position (analog to digital conversion). The other blocks of Figure 5 (presented in next section) are the control blocks, which are located in the PC (in the form of Matlab Simulink blocks).

4.1.2. Determination of the Control Blocks

4.1.2.1. "Position to Speed" Block

By setting a reference signal for the position with a sinusoidal variation, the desired speed has a sinusoidal variation. It is obtained simply by using a derivation block.

4.1.2.2. "Motor Simplified Electric Motor" Block

To control the motor, we must provide duty cycles for the four H-bridges of the inverter to the "PWM & power supply" block. To do this, the "Motor simplified electric model" block receives the currents, i_1 to i_4, as input and generates the duty cycles, k_1 to k_4. The content of this block is based on Equation (19) for phase number k:

$$U_k = R_k i_k + L_k \frac{di_k}{dt} + i_k \frac{dL_k}{dx} \frac{dx}{dt}$$

$$k_k = \frac{U_k}{U_{bus}}$$

(19)

We assume that the magnetic circuit of the motor has a linear behavior without saturation and that the phases are independent (no mutual inductance). This equation is commonly used in the works dealing with modeling and control of SRM [11,13].

The values of R, L and dL/dx are given in Section 3.1. The DC bus voltage, U_{bus}, corresponding to the supply voltage of the H-bridges is fixed at 30 V.

4.1.2.3. "Current Signal Generator" Block

The generation of currents, i_1 to i_4, is performed by the "Current signal generator" block. This block is an "S-function" of Matlab Simulink. The inputs are the desired total force, F, and the reference signal position, x. Figure 6 illustrates the current supply sequence required for a reference signal position.

Figure 6. Generation of the phase currents according to the reference position.
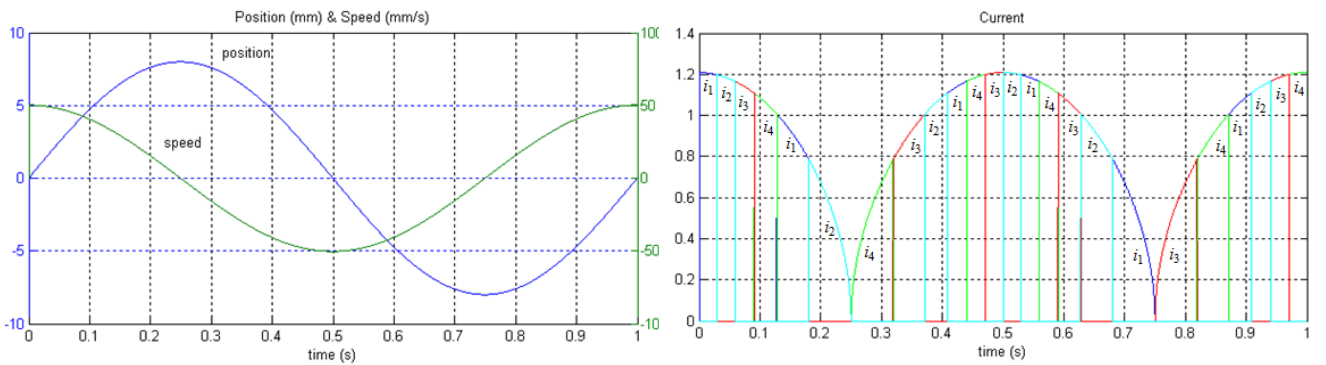
We can see that when the reference position increases (positive speed), the current supply sequence generated is in the order i_1, i_2, i_3, i_4 allowing movement of the mover in the direction of increasing x. On the contrary, when the reference position decreases (negative speed), the current supply sequence generated is in the order i_4, i_3, i_2, i_1, allowing movement of the mover in the direction of decreasing x.

The current amplitude is function of the desired force and is determined by:

$$F = \frac{1}{2} \frac{dL}{dx} i^2 \quad \Rightarrow \quad i = \sqrt{\frac{F}{\frac{1}{2} \frac{dL}{dx}}}$$

(20)

It is assumed here that only one phase is energized at a time, and only the phase supplied contributes to generating the desired force. Previous assumptions on the linearity, the non-saturation of the magnetic material and the independence of the phases are maintained. This equation is also used in work [14,15], which are related to the modeling of SRM.

4.1.2.4. "Speed to Force" Block

The desired total force, F, is generated from the reference speed, v, by the "Speed to force" block, which is chosen as a simple gain, K_{vF}, in order to simplify the control. Thus, the speed, v, and the desired total force, F, have the same evolution, which explains why the current waveform shown in Figure 6 is sinusoidal. A preliminary test was performed in order to determine the gain, K_{vF}. During this experiment, one phase of the motor was supplied by a square wave signal of 1 A, and the position of the mover was recorded (cf. Figure 7).

Figure 7. Preliminary test in order to determine K_{vF}.
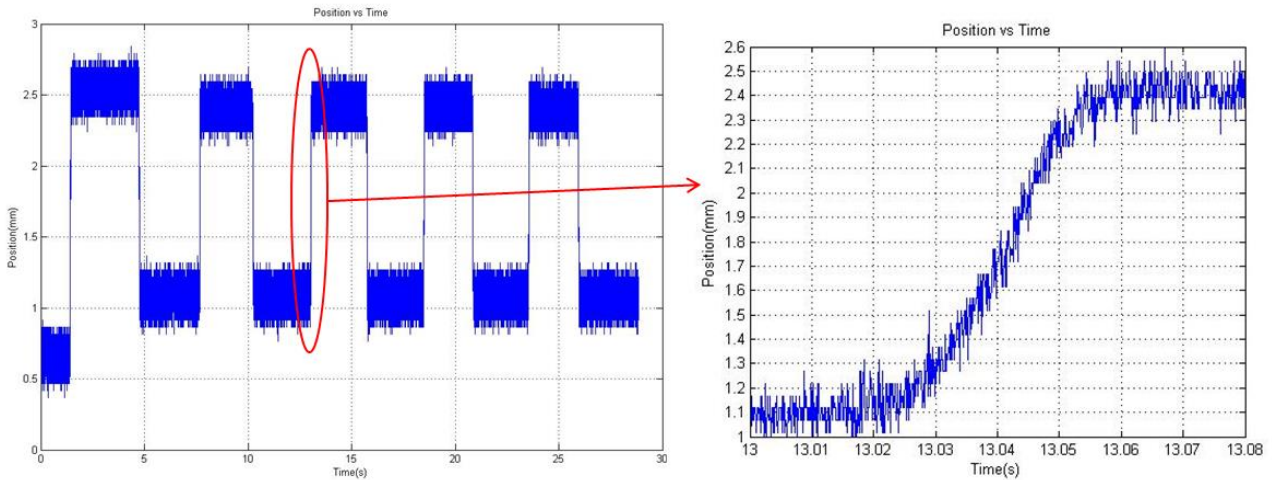
The determination of the slope of the curve, $x(t)$ (position *vs.* time curve zoomed in Figure 7), and the use of Equation (20) allowed us to determine the gain, $K_{vF} = 0.05$, where v is expressed in mm/s and F in N.

4.1.3. Modeling of the Motor with Matlab Simulink

4.1.3.1. Principle of Modeling

Figure 8 presents the modeling of the motor (modeling of the elements included in the dotted box of Figure 5). This will allow us to develop a correction for closed loop control.

The modeling of the motor is done in two steps. First, from the electrical equation, we construct the estimated currents, i_1^* to i_4^*, thanks to the "LSRM Electrical model" block. Then, from the mechanical equation, we construct the estimate of the measured position, x_m^*, thanks to the "LSRM Mechanical model" block.

**Figure 8.** Principle of modeling.
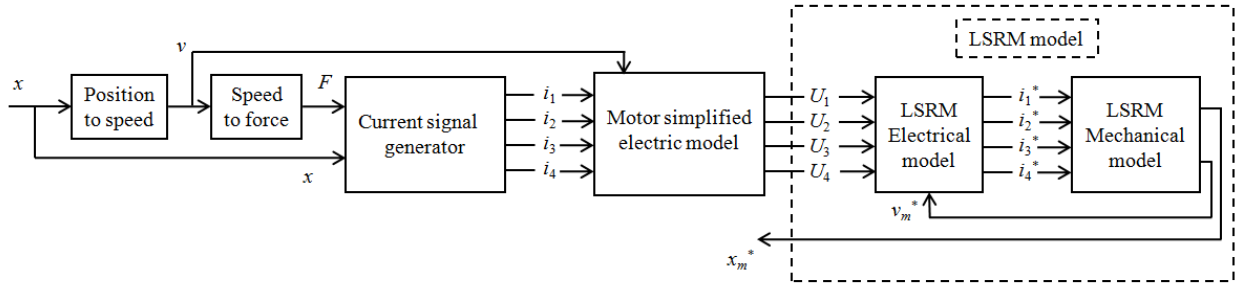
4.1.3.2. Electrical Modeling of the Motor

To model the motor phase number, k ($k = 1$ to 4), we can rely on Equation (19). Thus, for the reference voltage, U_k, the estimated current, i_k^*, can be reconstructed from:

$$\frac{di_k^*}{dt} = \frac{U_k}{L} - \left(\frac{R}{L} + \frac{1}{L}\frac{dL}{dx}v_m^*\right)i_k^*$$

(21)

To simplify, we assume that the rate of change of inductance with respect to the position, dL/dx, is constant and does not depend on the position of the mover (we will take the value given in Section 3.1). The estimated speed, v_m^*, comes from the next "LSRM Mechanical model" block. Figure 9 shows the block diagram of the electrical modeling of the phase, k.

Figure 9. Electrical modeling of one phase of the motor.
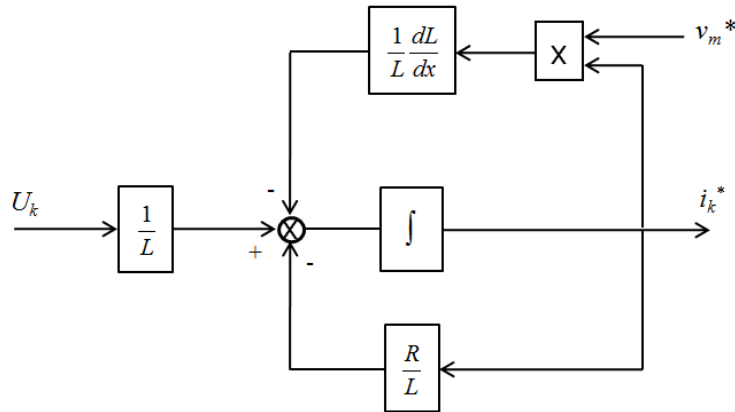
The "LSRM Electrical model" block of Figure 8 consists in reproducing the diagram shown in Figure 9 for the four phases of the motor.

4.1.3.3. Mechanical Modeling of the Motor

Each phase of the motor supplied by an input current, i_k^*, will produce a driving force, F_{mk}^*, according to:

$$F_{m_k}^* = \frac{1}{2}\frac{dL}{dx}i_k^{*2}$$

(22)

The sum for $k = 1$ to 4 of forces F_{mk}^* gives the estimated total motor force. As mentioned in Section 4.1.2, we assume a linear functioning of the magnetic circuit and a magnetic independence of the motor phases.

The mechanical equation governing the motion of the mover is given by:

$$\frac{d^2 x_m^*}{dt^2} = \frac{1}{m}\left(\sum_k F_{m_k}^* - f_s \cdot \text{Sign}\left(v_m^*\right)\right)$$

(23)

The dry friction force, f_s, and the mass, m, of the mover are given in Section 3.1. The viscous friction force is neglected. Figure 10 shows in block diagram form, the mechanical model of the motor based on Equation (23).

Figure 10. Mechanical modeling of the motor.
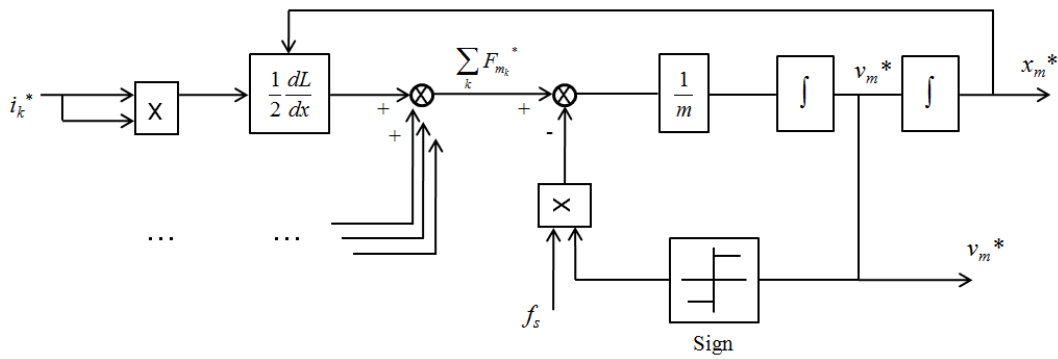
In order to have a realistic model, the rate of change of inductance is not taken with respect to the position dL/dx constant as in the "LSRM Electrical model" block. Once the estimated position of the mover, x_m^*, is calculated at time, t, the function, $g(x) = dL/dx$, takes into account this value to generate the position at the next time, $t + T_e$. It is important to define the function, $g(x)$, for the control and the modeling of the motor well. In [14,15], this function is used to elaborate the current control of an LSRM used for an elevator application.

The rate of change of inductance with respect to the position when supplying one single phase can be modeled by the inductance profile given in Figure 11. This assumes a linear variation of the inductance of phase number, k: L_k changes linearly between the values, L_u (unaligned teeth) and L_a (aligned teeth). Use of this type of model is common, for example, in work given in [11] and [13].

**Figure 11.** Inductance profiles of the four phases with respect to the position.
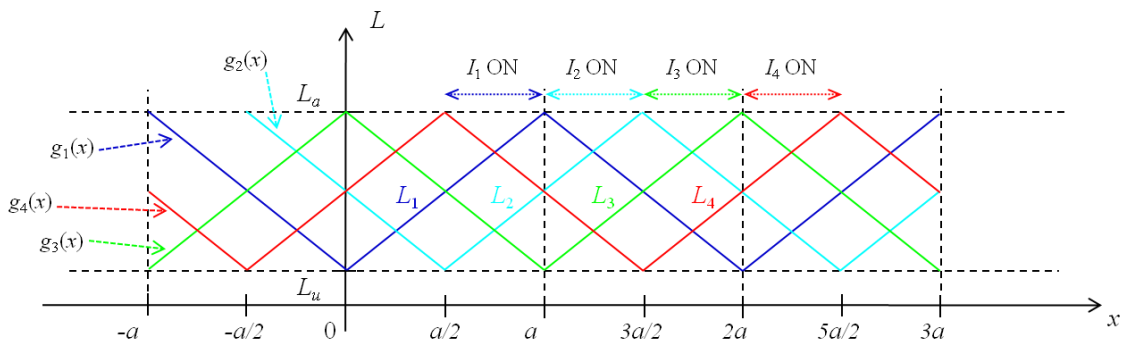
When the phases are supplied one after the other, taking care to supply one single phase at a time, the variations of inductances of phases 2, 3 and 4, namely L_2, L_3 and L_4, can be deduced from L_1 by translation. Figure 11 shows the inductance profiles, L_1 to L_4, with respect to the position and the current sequence power supply associated with it. As the rate of change of inductance is assumed to be linear, the functions, $g_k(x) = dL/dx_k$, are portions of straight lines. The possible values of $g_k(x)$ are real constants, shown in Table 4.

Table 4. Values of the functions, $g_k(x) = dL/dx_k$, with respect to the position, x (mod $2a$).

	$-a < x < -a/2$	$-a/2 < x < 0$	$0 < x < a/2$	$a/2 < x < a$	$a < x < 3a/2$	$3a/2 < x < 2a$
$g_1(x)$	−10/2.9	−10/2.9	10/2.9	10/2.9	−10/2.9	−10/2.9
$g_2(x)$	10/2.9	−10/2.9	−10/2.9	10/2.9	10/2.9	−10/2.9
$g_3(x)$	10/2.9	10/2.9	−10/2.9	-10/2.9	10/2.9	10/2.9
$g_4(x)$	−10/2.9	10/2.9	10/2.9	-10/2.9	−10/2.9	10/2.9

Finally, the mechanical modeling of the motor, *i.e.*, the content of the block "Mechanical LSRM model" of Figure 8, is given in Figure 12.

**Figure 12.** Content of the block diagram "LSRM (linear-switched reluctance motor) Mechanical model".
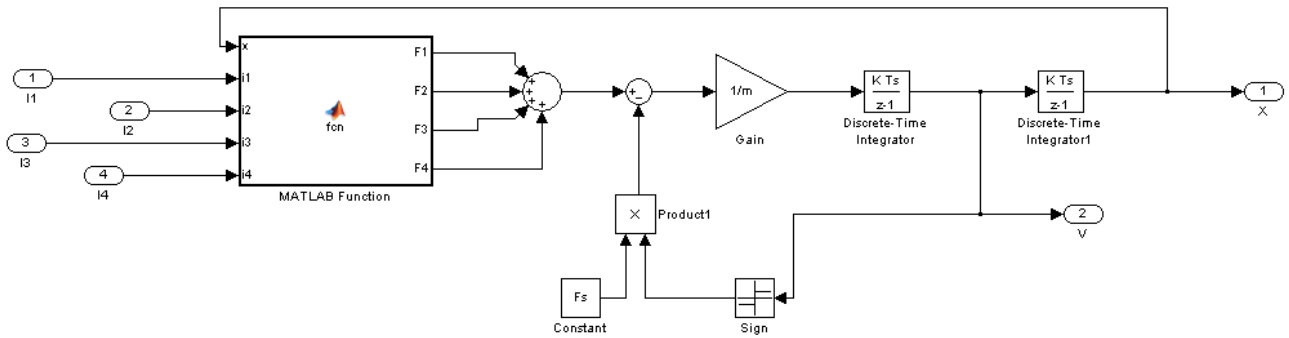
The "Matlab Function" calculates the values of $g_k(x)$ according to the position, x (cf. Table 4), and determines the effort of each phase, according to Equation (22).

The entire modeling of the motor can be improved by taking into account the values of $g_k(x)$ in the electrical modeling of the motor phase. For an inductance profile that is not linear without saturation, the modeling approach remains valid by giving the non-linear equation of the inductance profile with respect to the position.

4.1.4. Results of the Open Loop Control

The motor being modeled, Figure 13 illustrates the open loop response of the motor, x_m^*, to the desired position, x (10 mm amplitude and 2 Hz frequency).

**Figure 13.** Open loop configuration: input (position x) and output (position $x_m{}^*$) waveforms.
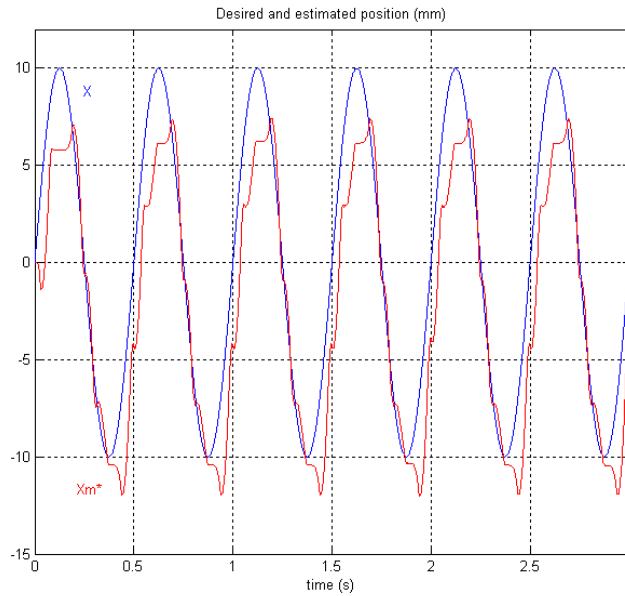
The steady state error requires setting up a closed loop control with an integral and derivative terms controller.

4.2. Closed Loop Control of the Motor

From Figure 8, the block diagram of the closed loop control of the motor can be established in Figure 14.

Figure 14. Closed loop control of the motor.
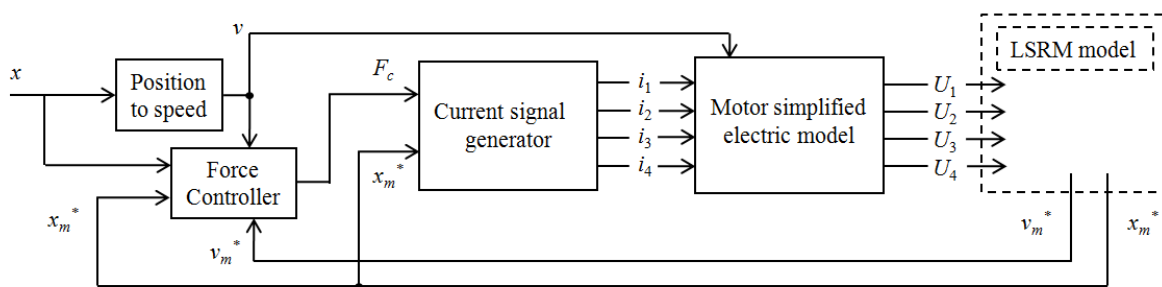
Thus, a block called "Force Controller" is implemented. From the reference position, x, and the estimated measured position, $x_m{}^*$, this block will generate the appropriate control effort. This corrector includes an integral action and an anticipatory action, called feed-forward, which allows for compensation of the tracking deviations during the speed ramps, and the integral action allows for compensation of the effects of disturbing efforts. To implement all these elements, we used the reference speed, v, and the estimated measured velocity, $v_m{}^*$.

The output of the "Force Controller" block is called the control force, F_c, which is provided to the "Current signal generator" block. We recall that this block must generate the current supply sequence, which allows the mover to achieve the desired position. It has the estimated measured position, $x_m{}^*$, as the second input. Figure 15 shows the implemented "Force Controller" block.

Figure 15. "Force Controller" block.
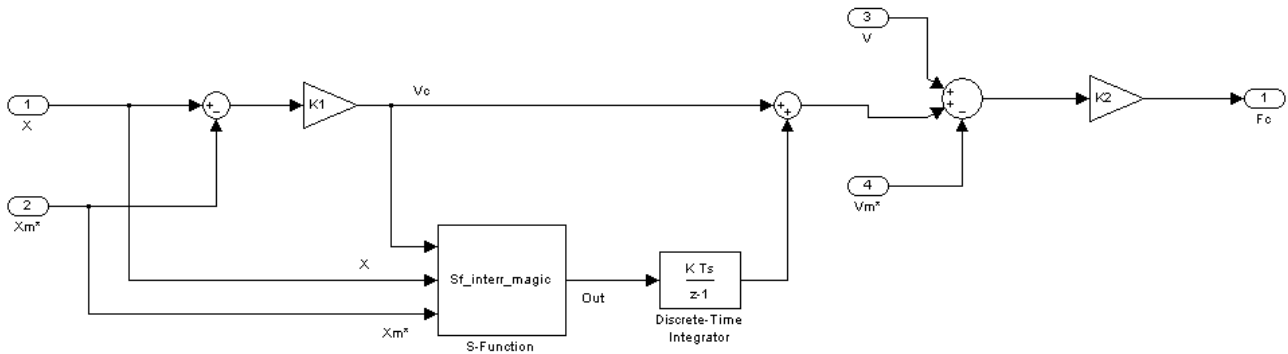
K_1 defines the proportional gain, which acts on the position error. The output of this gain is called the control speed, V_c. The integrator gain is chosen equal to ¼ of K_1 to obtain a proper integral action of the controller. Then, the control speed is corrected by an anticipatory (feed-forward) action. The gain, K_2, defines the proportional gain, which acts on the speed error. The output of the corrector is the control force, F_c. Upstream of the integrator, a "magic-switch" has been inserted. When the switch is open (out = 0), the integral action is held. This block is an "S-function" of Matlab Simulink and has x, x_m^* and the control speed, V_c, for inputs.

Figure 16. (a) Flow chart of the "magic-switch"; (b) Closed loop configuration: input (position x) and output (position x_m^*) waveforms.
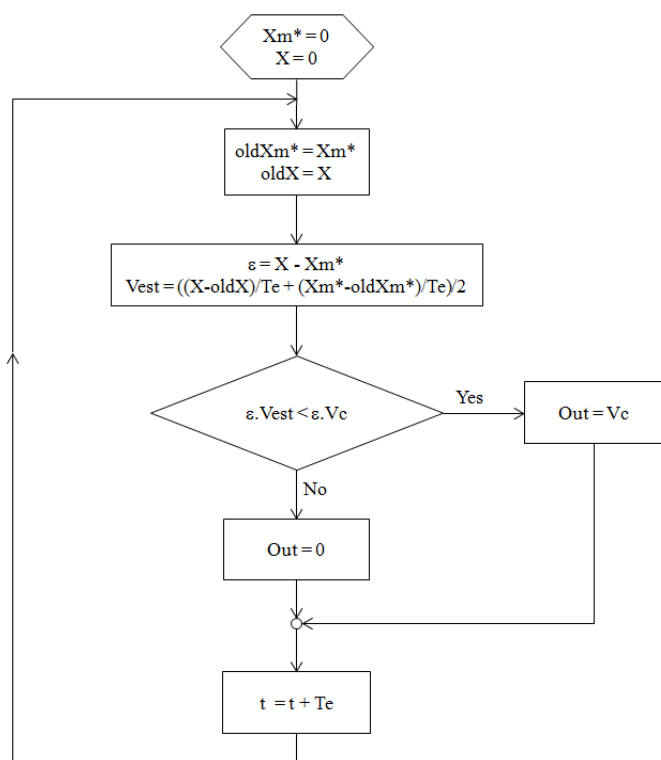
(a)
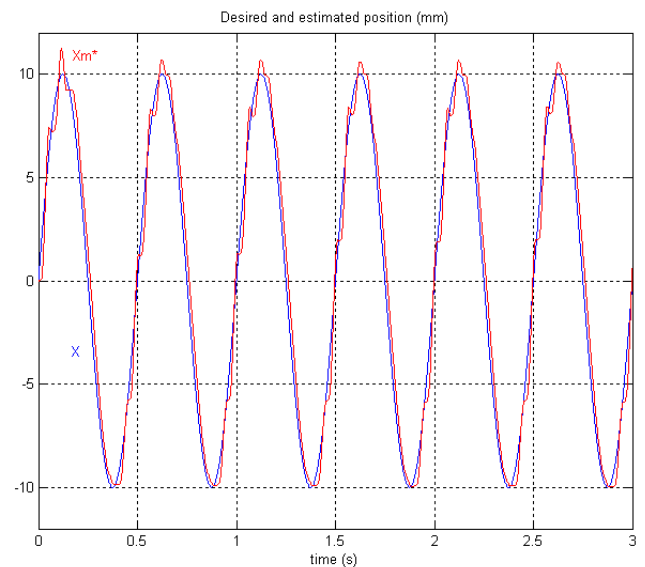
(b)

The flow chart of the S-function is presented in Figure 16(a). In principle, the speed error should not continue to be integrated to inflate the command when the dynamics of this error are such that it tends to disappear naturally, otherwise the extra control contributes to overshooting. To do this, signal V_c was compared to the estimated speed, V_{est}. When the estimated speed, V_{est}, is too rapid compared to V_c, then the switch is open (out = 0); otherwise, it will be closed (out = V_c).

Figure 16(b) shows the results of the closed loop control for the same input waveform, x, as in Section 4.1.4. We can see that the corrector cancels the steady state error. We can see also that the phase shift is very small between the two waveforms. The corrector thus ensures its function, and the measured output is very close to the input reference.

5. Conclusions

In this paper, we have presented a tubular linear-switched reluctance motor for a medical application. This actuator must provide a pulsatile pump operation for a ventricular assistance device. After describing the operating principle of this actuator, we presented the characteristics of the prototype actuator and the principle of position control. This control is based on a dSPACE control system associated with Matlab Simulink. A dedicated power supply based on a H-bridge inverter for the four phases of the machine has been developed.

A simplified model of the actuator was proposed, which can be generalized to a linear-switched reluctance motor for all applications. This modeling takes into account the variation of inductance with respect to the position and assumes an independence of the phases (and a linear behavior of the magnetic materials).

After this modeling, we present the open- and closed-loop position control of the actuator in Matlab Simulink. For the closed-loop control, a controller with an integral action and anticipatory action, called feed-forward, is implemented. We provide the implementation of a magic switch that prevents the integral action to inflate the command and that avoids overshoots of the output. The results obtained show that the use of a simplified model is satisfactory.

In the perspective of this work, a real control of the prototype under dSPACE based on the Simulink models already developed must be carried out.

References

1. DiGiorgi, P.L.; Naka, Y.; Oz, M.C. Left Ventricular Assist Devices. *Contemporary Cardiology: Surgical Management of Congestive Heart Failure*; Springer Humana Press: Totawa, NJ, USA, 2005; Chapter 7, pp. 155–189.
2. Blitz, A.; Fang, J.C. Ventricular Assist Devices and Total Artificial Hearts. *Contemporary Cardiology: Device Therapy in Heart Failure*; Springer Humana Press; Boston, MA, USA, 2009; Chapter 13, pp. 339–371.
3. Allen, G.S.; Murray, K.D.; Olsen D.B. The importance of pulsatile and non pulsatile flow in the design of blood pumps. *Artif. Organs* **1997**, *21*, 922–928.
4. Corda, J.; Skopljak, E. Linear Switched Reluctance Actuator. In Proceedings of 6th International Conference on Electrical Machines and Drives; Inspec/IEE: London, UK, 1993; pp. 535–539.

5. El Amraoui, L.; Gillon, F.; Vivier, S.; Brochet, P.; Benrejeb, M. Optimal Design Approach for Linear Tubular Machines. In Proceedings of IEEE International Conference on Systems Man and Cybernetics; IEEE: Danvers MA, USA, 2002; Volume 5, pp. 1–6.

6. Yamada, H.; Hamajima, T.; Xiang, S.; Nishizawa, N. Six-phase linear pulse motor as linear oscillatory actuator. *IEEE Trans. Mag.* **1987**, *MAG-23*, 2841–2843.

7. Llibre, J.F.; Martinez, N.; Nogarede, B.; Leprince, P. Linear Tubular Switched Reluctance Motor for heart assistance circulatory: Analytical and finite element modeling. In Proceedings of 10th International Workshop on Electronics, Control, Measurement and Signals (ECMS); IEEE: Danvers MA, USA, 2011; pp. 1–6.

8. Llibre, J.F.; Martinez, N.; Leprince, P.; Nogarède, B. Innovative Linear Pulsatile Pump for heart assistance circulatory. In Proceedings of The Eighth International Symposium on Linear Drives for Industry Applications (LDIA 2011), Eindhoven, The Netherlands, 3–6 July 2011.

9. Lee, B.-S.; Bae, H.-K.; Vijayraghavan, P.; Krishnan, R. Design of a linear switched reluctance machine. *IEEE Trans. Ind. Appl.* **2000**, *36*, 1571–1580.

10. Viorel, I.-A.; Hameyer, K.; Strete, L. Transverse flux tubular switched reluctance motor. In Proceedings of 11th International Conference on Optimization of Electrical and Electronic Equipment, OPTIM'08; IEEE: Danversp MA, USA, 2008; pp. 131–136.

11. Vasquez, H.; Parker, J.K. A new simplified mathematical model for a switched reluctance motor in a variable speed pumping application. *Mechatronics* **2004**, *14*, 1055–1068.

12. Vasquez, H.; Parker, J.K.; Haskew, T. Control of a 6/4 switched reluctance motor in a variable speed pumping application. *Mechatronics* **2005**, *15*, 1061–1071.

13. Krishnan R. *Switched Reluctance Motor Drives, Modeling, Simulation, Analysis, Design, and Applications*; CRC Press LCC: Boca Raton FL,USA, 2001; pp. 21–22.

14. Bae, H.-K.; Lee, B.-S.; Vijayraghavan, P.; Krishnan, R. A linear switched reluctance motor: converter and control. *IEEE Trans. Ind. Appl.* **2000**, *36*, 1351–1359.

15. Lim, H.S.; Krishnan, R.; Lobo, N.S. Design and control of a linear propulsion system for an elevator using linear switched reluctance motor drives. *IEEE Trans. Ind. Appl.* **2008**, *55*, 534–542.